Proceedings of the ASME 2021
International Design Engineering Technical Conferences and
Computers and Information in Engineering Conference
IDETC/CIE2021
August 17-20, 2021, Virtual, Online

DETC2021-67499

TOPOLOGY OPTIMIZATION WITH LOCALLY EVALUABLE COMPLEMENT SPACE CONNECTIVITY

Clinton B. Morris
Palo Alto Research Center
Palo Alto, CA

Amir M. Mirzendehdel
Palo Alto Research Center
Palo Alto, CA

Morad Behandish
Palo Alto Research Center
Palo Alto, CA

ABSTRACT

Enforcing connectivity of parts or their complement space during automated design is essential for various manufacturing and functional considerations such as removing powder, wiring internal components, and flowing internal coolant. The global nature of connectivity makes it difficult to incorporate into generative design methods that rely on local decision making, e.g., topology optimization (TO) algorithms whose update rules depend on the sensitivity of objective functions or constraints to locally change the design. Connectivity is commonly corrected for in a post-processing step, which may result in suboptimal designs. We propose a recasting of the connectivity constraint as a locally differentiable violation measure, defined as a "virtual" compliance, modeled after physical (e.g., thermal or structural) compliance. Such measures can be used within TO alongside other objective functions and constraints, using a weighted penalty scheme to navigate tradeoffs. By carefully specifying the boundary conditions of the virtual compliance problem, the designer can enforce connectivity between arbitrary regions of the part's complement space while satisfying a primary objective function in the TO loop. We demonstrate the effectiveness of our approach using both 2D and 3D examples, show its flexibility to consider multiple virtual domains, and confirm the benefits of considering connectivity in the design loop rather than enforcing it through post-processing.

1. INTRODUCTION

Topology optimization (TO) has emerged as a useful tool for generating complex geometries whose intricacies extend beyond the design capabilities of human designers. Generally, the material is laid out to optimize performance metrics determined by physics-based solvers based on numerical methods such as finite element analysis (FEA) [1,2]. The rise of TO as an automated design tool has coincided with a number of advancements in additive manufacturing (AM) which allow for the fabrication of complex geometries that were previously infeasible. The manufacturing freedom afforded by AM is not unlimited, though. AM imposes a new set of complex constraints on feasible material distributions and geometries [3,4]. Design for AM (DfAM) has focused on identifying and incorporating these constraints into design frameworks [5].

The incorporation of manufacturing constraints into the TO framework can be broadly classified into two approaches which are (1) post-processing optimized part after generation [6–8]; and (2) incorporating the constraints into the optimization loop [9–17]. The former generally results in suboptimal designs with respect to the optimized objective functions. For example, when considering powder removal after selective laser sintering (SLS), the part's optimized structural stiffness can be adversely affected after drilling holes to reach internal cavities to facilitate powder removal. Whenever possible, it is preferable to incorporate manufacturing constraints, such as connectivity between internal cavities and exterior space, into the optimization process, as opposed to introducing them later.

Connectivity of the complement space is only one example of a manufacturing constraint that must be considered to design functional parts. Other examples are lower-bounding minimum feature size [9], avoiding excessive overhangs to ensure self-supporting structures for fused deposition modeling (FDM) [12,18], and enforcing accessibility of the complement space by machine tools [19]. Incorporating these constraints into TO frameworks invariably hinges on the ability to locally evaluate them—or their violations, to penalize TO objective functions via continuous measures which are differentiable with respect to local changes in the design representation, such as density fields.

Connectivity is a global constraint which cannot be directly differentiated with respect to the design representation. Although

© 2021 by ASME

its global nature is problematic for its incorporation into a TO framework, enforcing connectivity of interior and exterior space (i.e., the part and its complement) is essential in multiple design contexts. For example, complement space connectivity (CSC) is important when designing parts requiring connected channels for powder removal after SLS, wiring across mounted components on the part surface or within its interior cavities, embedded conductors, coolant fluid flow, etc. Earlier studies [8,20] applied path finding algorithms that use combinatorial search such as A* [21] to find the shortest path between specified points within the interior of a part. However, such methods do not provide a locally evaluable measure to incorporate into TO, thus can only be used in post-processing leading to suboptimal parts.

Enforcing CSC in TO was considered in [16] to eliminate entrapped powder or resin for AM parts by ensuring that all internal cavities were connected to the boundaries of the design domain. The approach recasts the connectivity enforcement problem as a maximum "virtual" temperature minimization which leads to a simply-connected complement space—i.e., a design in which no standalone disconnected cavities are created. This approach was extended in [17] such that the location of internal cavities could be partially specified by imposing additional internal Dirichlet boundary conditions (fixed virtual temperatures) at locations where a cavity is desired. With this modified approach, the complement space is not necessarily simply-connected. The previous implementations, specifically the exclusive use of Dirichlet boundary conditions in the virtual problem, though, cannot ensure any two points are connected in the void space which is necessary when considering wiring between mounted and embedded components.

In this paper, we take a similar physics-inspired approach to enforcing CSC in TO that can be composed with other physics-based performance criteria such as structural stiffness or thermal conductance to enforce connectivity in the complement space between any two arbitrary points or regions. Our approach also relies on minimizing a "virtual" energy function or compliance of a hypothetical structure representing the complement space, but we utilize both Neumann *and* Dirichlet boundary conditions to enforce the desired connectivity in the complement space. A key advantage of our approach over combinatorial path finding (e.g., A*-based) methods is its ability to generate locally evaluable sensitivity fields to incorporate into gradient-descent TO. To this end, the part and its complement are implicitly represented by the super- and sub-level sets of a density field. At every TO iteration, we use the density field and its negation to evaluate physical and artificial stiffness matrices needed to compute the corresponding quantities of interest using an FEA solver. As a result, designers can specify both physics-based performance criteria and CSC constraints and assign relative weights to navigate the tradeoffs between them.

Our goal is to demonstrate that optimal topologies can be generated in such a way that two specified points or regions in the complement space are guaranteed to be path-connected. Our approach allows the designer to enforce CSC in anticipation of embedded components that must be connected (e.g., conductors) or channels to enable powder removal in SLS or accommodate wires/cables, while simultaneously optimizing for physics-based performance criteria. The approach can be in principle extended to combine CSC with other manufacturability constraints that are also locally evaluable and differentiable (e.g., accessibility, self-support, and accessible support) [19].

2.1 Contributions and Outline

The contributions of this paper are:

- introducing a general approach to enforce connectivity between arbitrary pairs of points in the design space during TO using "virtual" compliance measures;
- demonstrating the ability to enforce CSC while optimizing structural stiffness for representative 2D and 3D problems; and
- demonstrating the importance of incorporating CSC into the TO loop, as opposed to post-process modifications of optimized parts, to avoid suboptimal designs and enable navigating tradeoffs between the design criteria.

The remainder of the paper is organized as follows:

- Section 2 describes the problem formulation.
- Section 3 provides preliminary parameter studies to fine-tune the virtual compliance and its weighted combination with physics-based structural stiffness.
- Section 4 demonstrates how incorporating CSC constraints into the TO loop can change the part structure relative to TO without CSC constraints, in nontrivial ways.
- Section 5 provides a conclusion of what was presented and future directions.

2. CONNECTIVITY ENFORCEMENT FORMULATION

Figure 1 defines the terminology used in our approach.

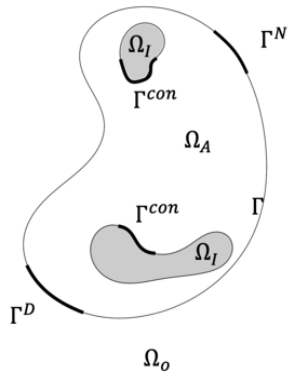


FIGURE 1: A general design domain considered in TO with connectivity enforcement among two or more Γ^N patches.

On the boundary Γ of the initial design domain Ω_0, one may specify physics-based Dirichlet and/or Neumann boundary conditions, Γ^D and Γ^N, respectively. In a mechanical context, they are displacements and loads, while in a thermal context,

 © 2021 by ASME

they are temperatures and heat fluxes. For density-based TO, a continuous density function, $\xi_\Omega: \Omega_0 \rightarrow [0,1]$ provides an implicit representation of a design $\Omega \subseteq \Omega_0$. In other words, the design domain Ω_0 is partitioned into active and inactive regions, Ω and $(\Omega_0 - \Omega)$, respectively, defined by super- and sub-level sets of the density field corresponding to prescribed thresholds, respectively. There are also connectivity boundaries, Γ^{con}, that must be connected in the complement space.

A typical (structural or thermal) TO problem (without CSC constraints) can be formulated as follows:

$$\begin{aligned} &\textit{minimize} && \varphi(\Omega) && (1a)\\ &\Omega \subseteq \Omega_0 && && \\ &\textit{such that} && [\boldsymbol{K}_\Omega][\boldsymbol{u}_\Omega] = [\boldsymbol{f}] && (1b)\\ & && V_\Omega \leq V_{\text{target}} && (1c) \end{aligned}$$

where $\varphi(\Omega) \in \mathrm{R}$ is the objective function (1a) over the design domain. The FEA arrays $[\boldsymbol{f}]$, $[\boldsymbol{u}_\Omega]$, and $[\boldsymbol{K}_\Omega]$ are the discretized external load vector, response vector, and stiffness matrix, respectively, whose relationship is constrained by (1b) resulting from physics-based governing equations. V_Ω is the volume of Ω that is upper-bounded in (1c) by a fixed budget V_{target}. In addition to these two constraints, we aim to introduce the CSC constraint in such a way that a local sensitivity field can be defined to penalize design modifications that compromise CSC.

To recast the CSC constraint into a locally differentiable form, we begin from a key observation that minimizing the (thermal or structural) compliance over a domain naturally leads to a path-connected structure joining the surfaces at which loads are applied (i.e., Neumann boundary conditions) to surfaces where the response to that load is fixed (i.e., Dirichlet boundary conditions). Intuitively, if such connectivity is violated, the part would undergo rigid motions, leading to zero-valued eigenvalues of the stiffness matrix used in the static equilibrium FEA.

Therefore, to enforce connectivity in the complement space, we formulate a virtual compliance function over the design space, for the hypothetical response of a virtual part to virtual loads applied at Γ^{con}:

$$c_\Omega^{con} = [\boldsymbol{f}^{\boldsymbol{con}}]^T[\boldsymbol{u}_\Omega^{\boldsymbol{con}}] = [\boldsymbol{u}_\Omega^{\boldsymbol{con}}]^T[\boldsymbol{K}_\Omega^{\boldsymbol{con}}][\boldsymbol{u}_\Omega^{\boldsymbol{con}}] \qquad (2)$$

where, $[\boldsymbol{f}^{\boldsymbol{con}}]$, $[\boldsymbol{u}_\Omega^{\boldsymbol{con}}]$, and $[\boldsymbol{K}_\Omega^{\boldsymbol{con}}]$ are the virtual discretized external load vector, displacement vector, and stiffness matrix, respectively. A variety of virtual physics-based interpretations could be selected, e.g., thermal physics would lead to scalar values for the load and response (namely, heat fluxes and temperatures) whereas structural physics would lead to vector values (namely, forces and displacement). The impact of the selected virtual physics will be explored later. In general, we specify Neumann boundary conditions at one region of Γ^{con}, referred to as the 'inlet', and a Dirichlet boundary condition at another region, referred to as the 'outlet'. Figure 2 provides an illustration for how the original domain of Fig. 1 translates to our virtual compliance problem using structural physics for (2).

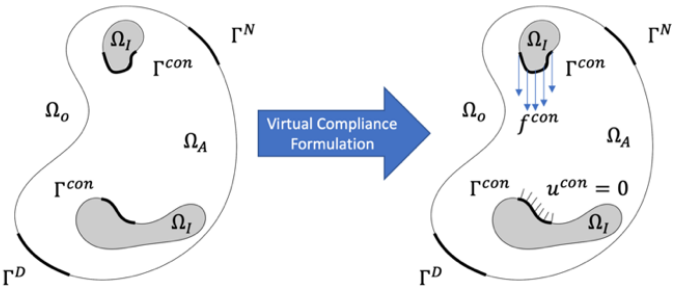


FIGURE 2: The CSC constraints translated into virtual boundary conditions for virtual compliance formulation.

With the CSC constraint recast into a locally differentiable form, we return to the primary TO problem to introduce how the virtual connectivity is incorporated. To begin, we ignore the connectivity constraint to form the prototypical Lagrangian, L_Ω for the primary TO:

$$L_\Omega = \varphi(\Omega) + \lambda_1\left(\frac{V_\Omega}{V_{target}} - 1\right) + [\boldsymbol{\lambda_2}]^T([\boldsymbol{K}_\Omega][\boldsymbol{u}_\Omega] - [\boldsymbol{f}]) \quad (3)$$

By performing a representation-agnostic differentiation of the Lagrangian with respect to Ω, we obtain

$$\boldsymbol{L}'_\Omega = \left(\left[\frac{\partial\varphi(\Omega)}{\partial \boldsymbol{u}}\right] + [\boldsymbol{\lambda_2}]^T[\boldsymbol{K}_\Omega]\right)[\boldsymbol{u}'_\Omega] + \lambda_1\frac{V'_\Omega}{V_{target}} + [\boldsymbol{\lambda_2}]^T[\boldsymbol{K}'_\Omega][\boldsymbol{u}_\Omega] \qquad (4)$$

Computation of $[\boldsymbol{u}'_\Omega]$ is challenging, but (4) can be simplified by selecting $[\boldsymbol{\lambda_2}]$, one of the Lagrange multipliers, as the solution to the adjoint problem to obtain:

$$\boldsymbol{L}'_\Omega = \lambda_1\frac{V'_\Omega}{V_{target}} - \left([\boldsymbol{K}_\Omega]^{-1}\left[\frac{\partial\varphi(\Omega)}{\partial \boldsymbol{u}}\right]\right)^T[\boldsymbol{K}'_\Omega][\boldsymbol{u}_\Omega] \qquad (5)$$

If the objective is the compliance, $\varphi(\Omega) \coloneqq [\boldsymbol{f}]^T[\boldsymbol{u}_\Omega]$, then $[\boldsymbol{\lambda_2}]$ reduces to $-[\boldsymbol{u}_\Omega]$ because compliance is self-adjoint [2].

Let $S_\varphi: \Omega_0 \rightarrow \mathbb{R}$ represent the sensitivity field of the primary objective, that is the field provided by the second term on the RHS of (5). We can define a similar field $S_{con}: \Omega_0 \rightarrow \mathbb{R}$ for the virtual compliance used to quantify the violation of the CSC constraint. We use a weighted convex sum of the two fields, in which the weighting factor $0 \leq w_{con} \leq 1$ controls the degree to which the CSC constraint is enforced and can either be static or dynamically changed during TO iterations:

$$S_\Omega \coloneqq (1 - w_{con})S_\varphi + w_{con}S_{con} \qquad (6)$$

where $S_\varphi = -[\boldsymbol{u}_\Omega]^T[\boldsymbol{K}'_\Omega][\boldsymbol{u}_\Omega]$ and $S_{con} = -[\boldsymbol{u}_\Omega^{\boldsymbol{con}}]^T[\boldsymbol{K}_\Omega^{\boldsymbol{con}'}][\boldsymbol{u}_\Omega^{\boldsymbol{con}}]$.

© 2021 by ASME

With the formulation provided, we provide the CSC constrained formulation below for clarity where c_Ω^φ is the primary objective.

$$\begin{aligned} &\textit{minimize} && (1-w_{con})c_\Omega^\varphi + w_{con}c_\Omega^{con} && (7a)\\ &\Omega \subseteq \Omega_0 && && \\ &\textit{such that} && [\boldsymbol{K}_\Omega][\boldsymbol{u}_\Omega] = [\boldsymbol{f}] && (7b)\\ & && [\boldsymbol{K}_\Omega^{con}][\boldsymbol{u}_\Omega^{con}] = [\boldsymbol{f}] && (7c)\\ & && V_\Omega \le V_{\text{target}} && (7d) \end{aligned}$$

To generate results for this paper and provide more detail on how CSC is enforced, we use a density-based approach, namely the solid isotropic material penalization (SIMP) approach [22], although the idea is, in principle, extensible to other (e.g., level-set) TO methods. The primary objective, is to minimize the structural compliance while enforcing connectivity in the complement space between two regions. We start with the density field, $\xi_\Omega: \Omega_0 \rightarrow [0,1]$ that maps every point $x \in \Omega_0$ in the design domain to a density value $\xi_\Omega(x) \in [0,1]$. The discretization of the density field $[\xi_\Omega]$, is a finite array of design variables in the range $[0,1]$ to be optimized. To compute the elasticity for intermediate densities, we first use a Heaviside projection [2]:

$$\rho_0(x) = 1 - e^{-\beta\xi_\Omega(x)} + \xi_\Omega(x)e^{-\beta} \qquad (8)$$

in which we use $\beta := 2$ for 2D and $\beta := 10$ for 3D examples. The discretized density field $[\boldsymbol{\rho_0}]$ can be mapped to a discretized elasticity field (e.g., elemental Young's modulus) as follows:

$$[\boldsymbol{E}] = E_{min}[\boldsymbol{1}] + (E_{max} - E_{min})[\boldsymbol{\rho_\Omega}]^p \qquad (9)$$

where the elasticity bounds E_{min} and E_{max} and the penalization parameter $p > 1$ are constants. With the elemental Young's modulus defined, the elemental stiffness (which depends on the physics), and global stiffness matrix $[\boldsymbol{K_\Omega}]$ can also be formed in a standard fashion as shown in [22].

The virtual stiffness used to quantify the virtual compliance for CSC is defined in a similar fashion where the material interpolation scheme is used to determine the global stiffness matrix, $[\boldsymbol{K_\Omega^{con}}]$ that depends on the desired virtual physics. The exception is that it uses the negation of the density field that implicitly represents the complement space:

$$[\boldsymbol{E^{con}}] = E_{min}[\boldsymbol{1}] + (E_{max} - E_{min})[\boldsymbol{1} - \boldsymbol{\rho_\Omega}]^p \qquad (10)$$

The impact of this negation will appear in the sensitivity field in (6) where the sign of S_{con} will be negated due to the chain rule applied to $[\boldsymbol{K_\Omega^{con'}}]$ term. We use the method of moving asymptotes (MMA) [23] to update the discretized density during optimization rather than optimality criteria (OC), as the former provides a more straightforward path to optimizing non-convex functions. Additionally, it should be noted that the artificial material properties used in (10) need not be the same as those used for the primary problem.

Figure 3 illustrates the TO workflow with CSC enforcement. In every design iteration, two FEA instances are called using the same or different solvers to compute the relevant responses for physical and virtual problems. These responses are then used to calculate the primary objective function and sensitivity fields, which are used in an update scheme, in this case MMA, to update the design iteratively.

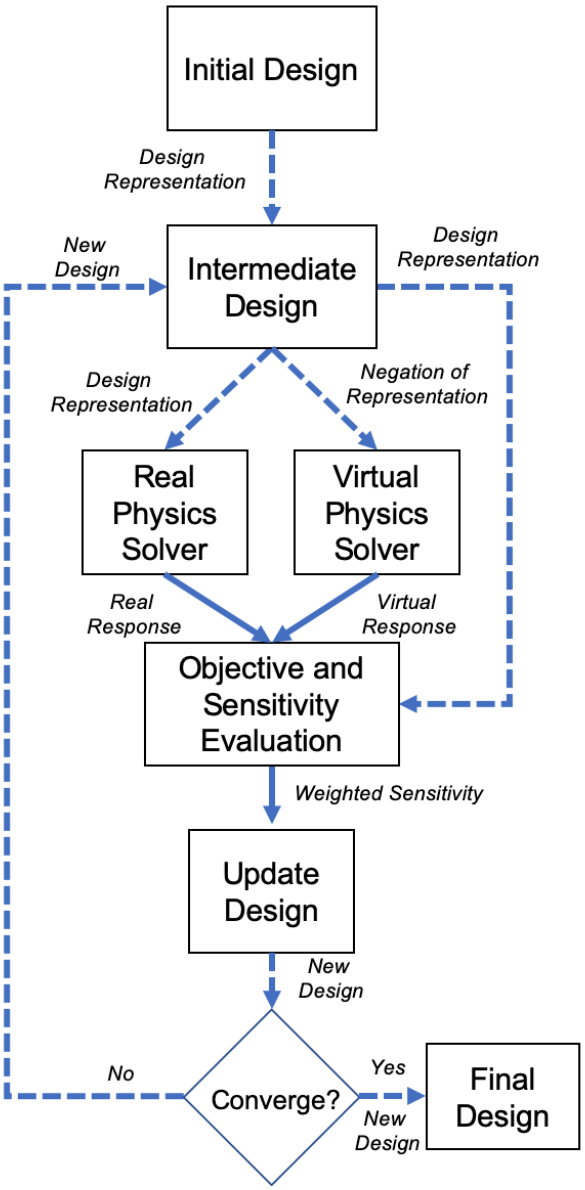


FIGURE 3: TO workflow for incorporating CSC constraints.

© 2021 by ASME

3. INFLUENCE OF DOMAIN ON CONNECTIVITY ENFORCEMENT

From the formulation of connectivity enforcement, there are multiple parameters that can influence the connectivity results. The most interesting is the virtual physics domain on which the virtual (e.g., thermal or mechanical) compliance is formulated. While previous work on connectivity enforcement focused on the thermal formulation, we investigate the impact of different physics on CSC enforcement within our framework.

We performed three studies to both demonstrate the effectiveness of our approach for CSC enforcement and compare the impacts of each virtual physics domain. All three studies were performed on the same or slightly modified design domain shown in Fig. 4. The inlet location for CSC is always on the boundary of the circular inactive domain directly above its center but the outlet is not shown because it will vary from study to study. The inactive domain is always void in this work. For all tests, the material properties and penalizations used are provided by Tab. 1 as well as the relevant parameters that were fixed for all case studies.

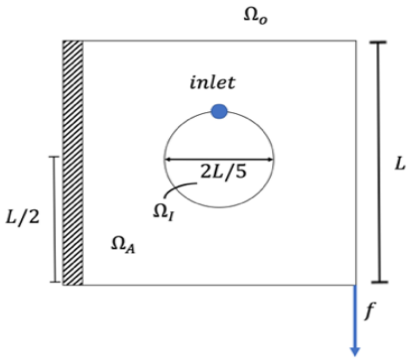


FIGURE 4: Cantilever beam example with a fixed inlet and different outlets used for parameter studies.

Parameter	Value
E_{max}	1
E_{min}	1E-9
p	3
$\mathrm{P}^{\mathrm{CON}}$	5
β	2

TABLE 1: Relevant parameters (fixed for all case studies).

The first study was used to ensure the approach enforced connectivity between inlets and outlets regardless of virtual physics. Therefore, the domain shown in Fig. 5 was used where the location of the inlet was fixed and the location of the outlet was varied. To minimize confounding effects, this study does not consider the primary objective function based on the physical performance of the cantilevered structure, i.e., assumes that CSC is the only design criterion, which corresponds to $w_{con} = 1$ in (7).

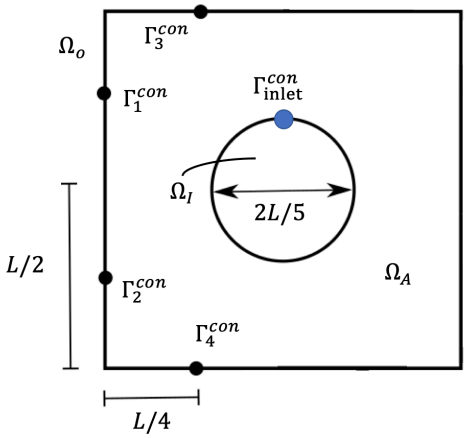


FIGURE 5: Diagram showing the location of eight different outlets used to validate approach.

We used both thermal and structural formulations of the virtual compliance to enforce CSC. For the former, we applied a unit flux at the inlet shown in Fig. 5, whereas for the latter, we applied a unit force in the negative Y-direction at the inlet. For both variants, we applied homogenous Dirichlet boundary conditions to each of the 4 indicated locations and used a constant target volume fraction of 0.85. The length of the Dirichlet boundary condition was $0.05L$ to ensure stability. The results of the study are shown in Fig. 6 where the domain was a 400×400 voxel mesh. Blue indicates dense elements, white indicates active void elements, and red elements are inactive void elements. The red elements can be viewed as an embedded component as well but do not contribute to the primary or virtual compliance. These colors are consistent across all figures showing TO results for the remainder of the paper unless indicated otherwise.

© 2021 by ASME

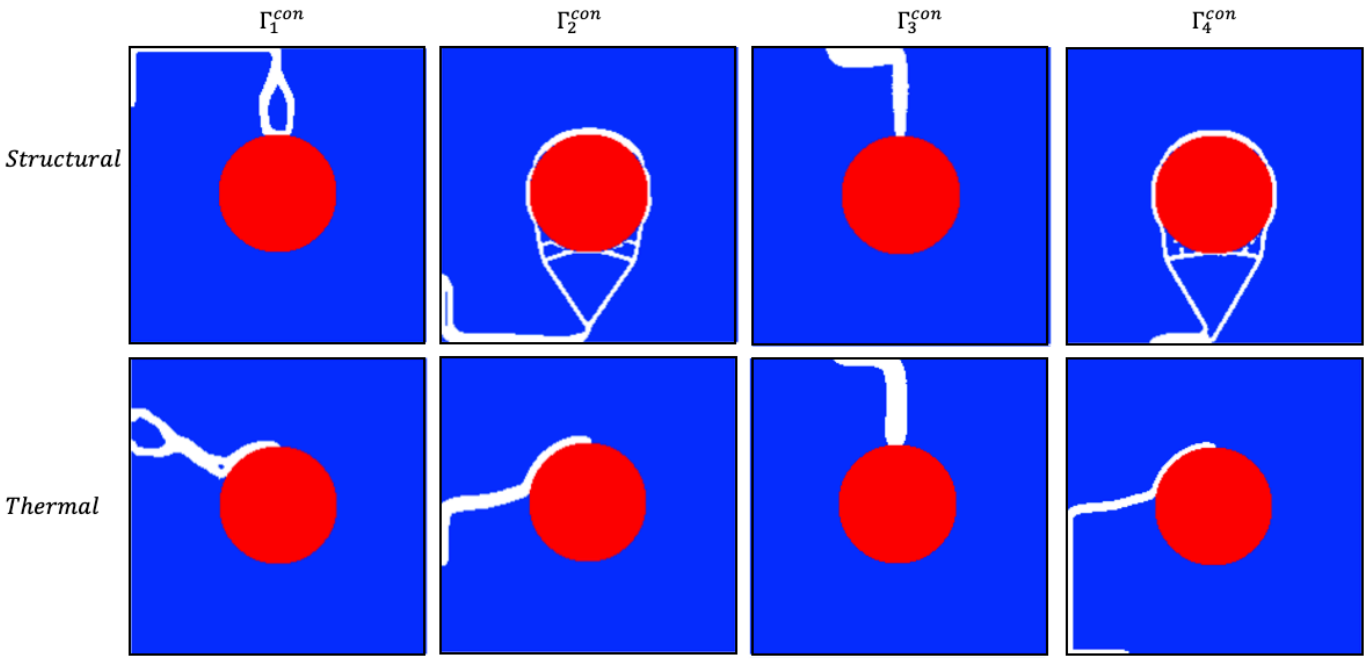


FIGURE 6: Results from the first parameter study where the outlet location was varied to the four indicated locations. The top row was generated using a virtual structural compliance while the bottom row utilized a thermal compliance. Blue indicates a dense region, red is the void inactive domain, and white is the void region

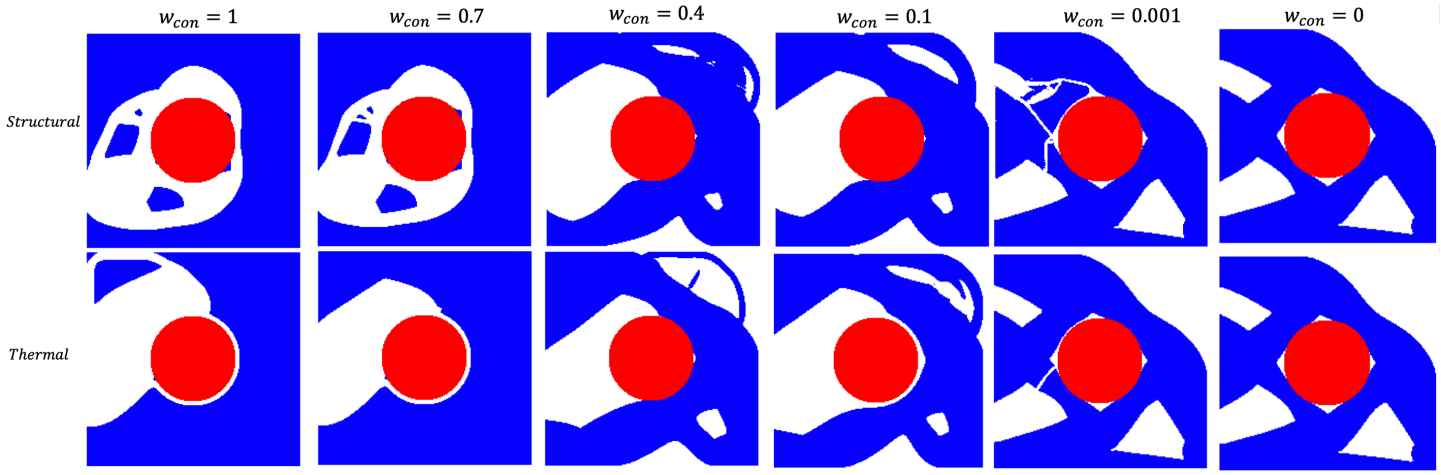


FIGURE 7: Results from the second parameter study where the connectivity weight was varied. The top row was generated using a virtual structural compliance while the bottom row utilized a thermal compliance**.** Blue indicates a dense region, red is the inactive domain, and white is the void region

As shown in Fig. 6, CSC is enforced in the void, white space between inlets and outlets regardless of the position of the outlet and regardless of the virtual physics used. Unsurprisingly, the resultant geometries differ across the virtual physics given the same inlet and outlet locations due to the fundamentally different physics being captured by (7c). This case study in which $w_{con} = 1$ is equivalent to minimizing the structural or thermal compliance for a hypothetical material in the complement space.

Additionally, the location of the outlet (and inlet) drastically influence the final geometry of the part regardless of physics. If the location of the inlets and outlet is not defined *a priori* or can vary over some region, then it is unclear what the best locations are. Including the inlet/outlet locations as design variable in the optimization loop is an area of future work.

For the second case study, the purpose was to understand the impact of $0 < w_{con} < 1$ on the optimized shape for both virtual domains. Therefore, the configuration shown in Fig. 5, where the outlet is located at Γ_2^{con} was used while varying w_{con}. The selected values for w_{con} were 1, 0.7, 0.4, 0.1, 1E-3, and 0, and the volume fraction target was 0.6. The resulting shapes are shown in Fig. 7.

It is clear that increasing w_{con} affects the resulting shape. As expected, when CSC is not enforced, the inlet and outlet are not connected. Once CSC is enforced, even for small $w_{con} > 0$,

© 2021 by ASME

the inlet and outlets are connected for both virtual physics, although the means by which connectivity is enforced for smaller weights varies significantly between the two virtual domains. It appears that the thermal formulation leads to more direct paths, while the structural domain favors paths with diverging and converging routes. As shown in Fig. 7, these complex routes can can result in disconnected (floating) blue regions. The avoidance of these disconnected regions could potentially be accomplished through filtering. As w_{con} is increased to more moderate values 0.1-0.6, the geometries are more similar across physics. For larger values of w_{con}, the geometries diverge once again, favoring the solutions of compliance minimization in the complement space.

Additionally, we computed the structural compliance of each structure as shown in Tab. 2 with the associated weights and virtual physics. The values are provided as ratios of the compliance to that of the extreme case $w_{con} = 0$. Note that higher values of the complian

	Compliance ratio	
w_{con}	Structural	Thermal
1	2.03	1.86
0.7	1.48	1.55
0.4	1.38	1.34
0.1	1.24	1.15
0.001	1.00	1.00
0	1.00	1.00

TABLE 2: Compliance values for a variety of connectivity weights for enforcing CSC with two different virtual physics.

As w_{con} is increased, the primary structural compliance also increased. There is good agreement between the values across the virtual physics domains, indicating that the selected physics do not drastically affect the performance with respect to the primary objective function, although, this may not always be the case.

The final case study was to understand the behavior of the approach when an obstacle is introduced along with a low void material budget (high target volume fraction). The domain is shown in Fig. 8 where an additional inactive domain is added to the domain of Fig. 4 and the outlet is specified by Γ^{con}.

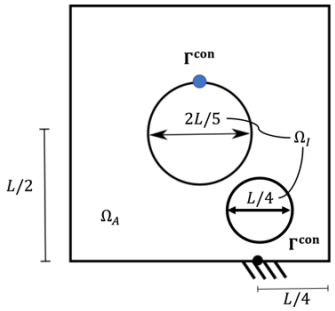


FIGURE 8: Domain (left) and results (right) where connectivity was enforced with an obstacle between inlet and outlet.

Once again, we considered no primary physical criterion for connectivity enforcement and the results are shown in Fig. 9 where we used a desired volume fraction of 0.85.

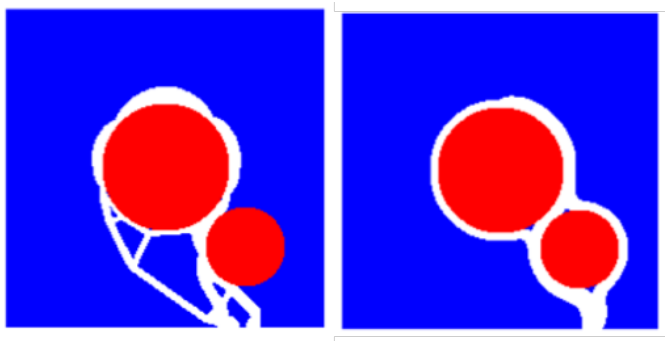


FIGURE 9: Results from the third parameter study where an obstacle and low complement space volume budget were used. The structural compliance for ensuring CSC is shown on left and the thermal compliance is shown on the right.

Once again, we see both domains enforce connectivity, but the thermal domain creates more direct paths while the structural domain creates more complex paths. It should be noted that the computational complexity of solving the thermal finite element problem is significantly smaller than that of the structural domain due to the number of degrees of freedom. It seems then, that the virtual thermal domain is likely preferable to the structural domain unless there is a need for complex pathways.

4. ENFORCING CONNECTIVTY DURING DESIGN GENERATION

This section presents the impact of incorporating CSC into the TO loop on the shape/topology and physical performance of structurally optimized parts compared to unconstrained TO followed by post-process correction for CSC. We show that that latter may result in designs with drastically lower performance.

The first example is in 2D where we used the domain shown in Fig. 10. The design is like a cantilevered beam but only half of the domain on the left-hand side is fixed to the wall and the load is applied at the midpoint of the right-hand face. The desired CSC is between a point on the inactive domain boundary and a point slightly below the applied force. This example can represent an embedded circular component that needs wiring to connect to an external point near the applied force. The inlet is the point on the inactive domain boundary and the outlet is the other points. Both thermal and structural formulations are once again are considered for virtual compliance. For the thermal domain a unit flux is applied at the inlet and for the structural domain a unit downward force in the y-direction is applied at the inlet for connectivity enforcements. This domain is intended to represent an embedded component that needs to be connected to another component mounted on the right-hand boundary.

© 2021 by ASME

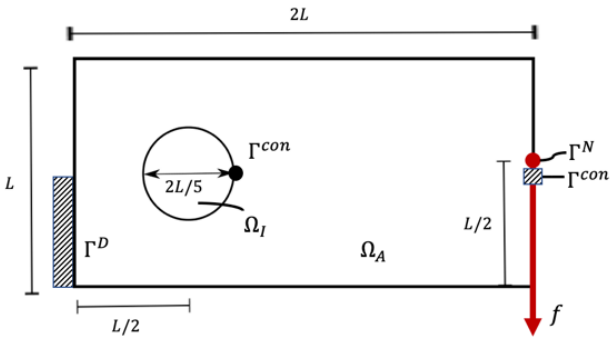


FIGURE 10: Illustration of the domain used for a structural compliance minimization problem with CSC enforcement.

With the domain established, we selected a target volume fraction of 0.25 and generated 4 optimized design on a 400×200 voxel mesh. The first design (top left) did not consider connectivity ($w_{con} = 0$). The second design (top right) was generated by removing material between inlet and outlet after generating a structure in which connectivity is not enforced ($w_{con} = 0$). The third (bottom left) and fourth (bottom right) designs were generated using $w_{con} = 0.9$ using both thermal and structural virtual physics for enforcing CSC, respectively. The results are shown in Fig. 11. Black indicates dense elements, white indicates active void elements, and red elements are inactive, void elements.

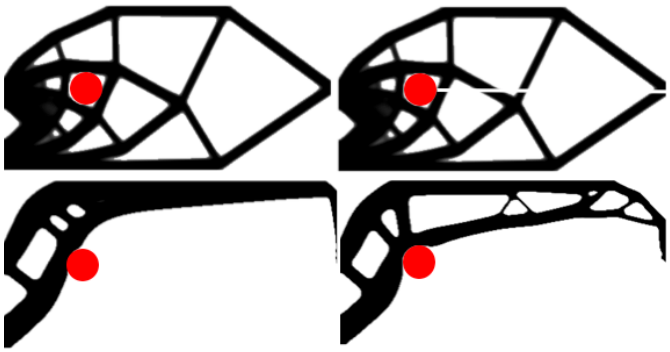


FIGURE 11: Results of TO without CSC enforcement (top left), with post-process correction for CSC (top right), with CSC enforcement in the TO loop using thermal compliance (bottom left), and structural compliance (bottom right).

Figure 11 shows that without enforcing CSC, the desired points are not connected in the complement space. Once connectivity is considered though, a path in the complement space is formed which dramatically changes the shape of the structure. Once again, the shapes are similar when connectivity is enforced regardless of the virtual physics used for CSC. When comparing the compliances, the unconstrained TO's outcome is 5.22 and 4.68 times stiffer compared to the CSC constrained TO's outcomes, using virtual thermal and structural compliance in the TO loop, respectively. While the change in compliance is significant, the unconstrained structure is 3900 times stiffer than the post-processed structure where connectivity was enforced by removing a path between inlet and outlet after TO. To ensure structural integrity, it is necessary to consider the connectivity constraint in the design loop.

The next example is another 2D example where we used the domain shown in Fig. 12. The design is like a cantilevered beam but only half of the domain on the left-hand side is fixed to the wall and the load is applied at the bottom right corner. The desired connectivity is between two points on the boundaries of two inactive domains. The inlet is the point on the left inactive domain boundary and the outlet is the other point. This domain is intended to represent two embedded components needing to be internally connected within a cantilevered structure.

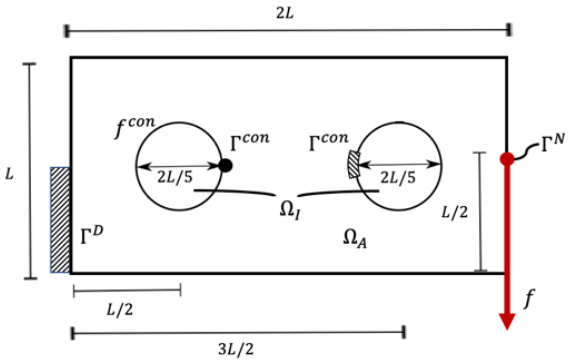


FIGURE 12: Illustration of the domain used for a structural compliance minimization problem with CSC enforcement between two embedded components.

We selected a target volume fraction of 0.5 and, once again, four designs were generated on a 400×200 voxel mesh. The first design did not consider connectivity ($w_{con} = 0$). The second design was generated by removing material between inlet and outlet after generating a structure in which connectivity is not enforced ($w_{con} = 0$). The third and fourth designs were generated using $w_{con} = 0.5$ using both thermal and structural virtual physics for enforcing CSC, respectively. The results are shown in Fig. 13 where black indicates dense elements, white indicates active void elements, and red elements are inactive void elements.

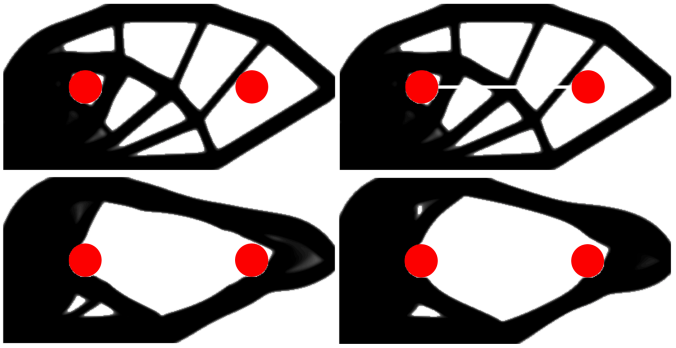


FIGURE 13: Results of TO without CSC enforcement (top left), with post-process correction for CSC (top right), with CSC enforcement in the TO loop using thermal compliance (bottom left), and structural compliance (bottom right**).**

© 2021 by ASME

Figure 13 shows that without enforcing CSC, the desired points are not connected in the complement space. Once connectivity is considered though, a path in the complement space is formed which changes the shape of the structure. Matching intuition, the structural features between the two inactive regions were eliminated. Interestingly, the removal of these members resulted in multiple other changes in shape to compensate for the decrease in rigidity and the addition material budget for both CSC constrained structures.

To once again demonstrate the need to enforce CSC in the design loop, the compliances were computed for all of the structures show in Fig. 13. The normalized compliance relative to the compliance of the unconstrained and unprocessed structure, c_0, for all four structures is provided by Tab. 3.

	c/c_0
No post-process	1.00
$w_{con} = 0$, Post-process	224.74
$w_{con} = 0.05$, Thermal	1.14
$w_{con} = 0.05$, Structural	1.24

TABLE 3: Normalized compliance results for the three generated topologies.

Table 3 shows that the stiffness is vastly inferior for the post-processed part while the stiffness is only slightly reduced when connectivity is considered in the design loop.

The next example demonstrates the effectiveness of the approach on 3D structural problems where we used the domain shown in Fig. 14. The design is a cantilevered beam where the load is applied at the indicated locations. The design has two inactive domains. The first inactive region is an embedded cylinder that is void except for voxels on the surface of the design domain. The second inactive domain is on the indicated boundary of the design domain and is enforced to be fully dense. There is a region within the second inactive domain that is active, though, and this serves as the outlet for an enforced connection to the inlet on the surface of the voided region. This region is intended to represent an embedded component needing to be connected to another component mounted on the boundary.

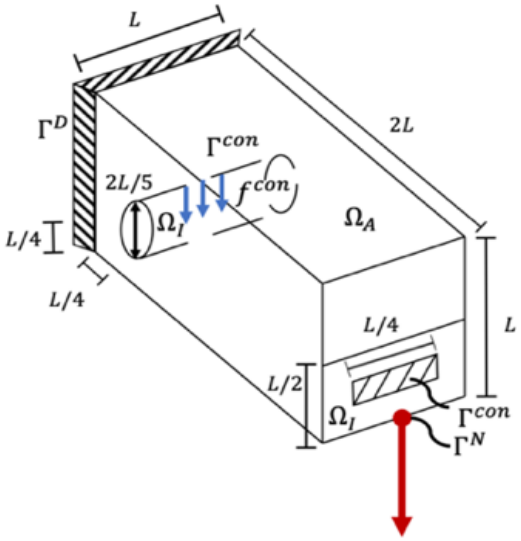


FIGURE 14: Illustration of the domain used for a structural compliance minimization problem with connectivity enforcement in 3D.

We used a target volume fraction of 0.3 and generated designs on a 100 x 50 x 50 voxel mesh. We varied w_{con} at the following values: 0, 0.1, 0.5, and 0.8. For each weight, we used both thermal and structural virtual physics to enforce CSC. The resulting parts as well as various views are shown in Fig. 15.

© 2021 by ASME

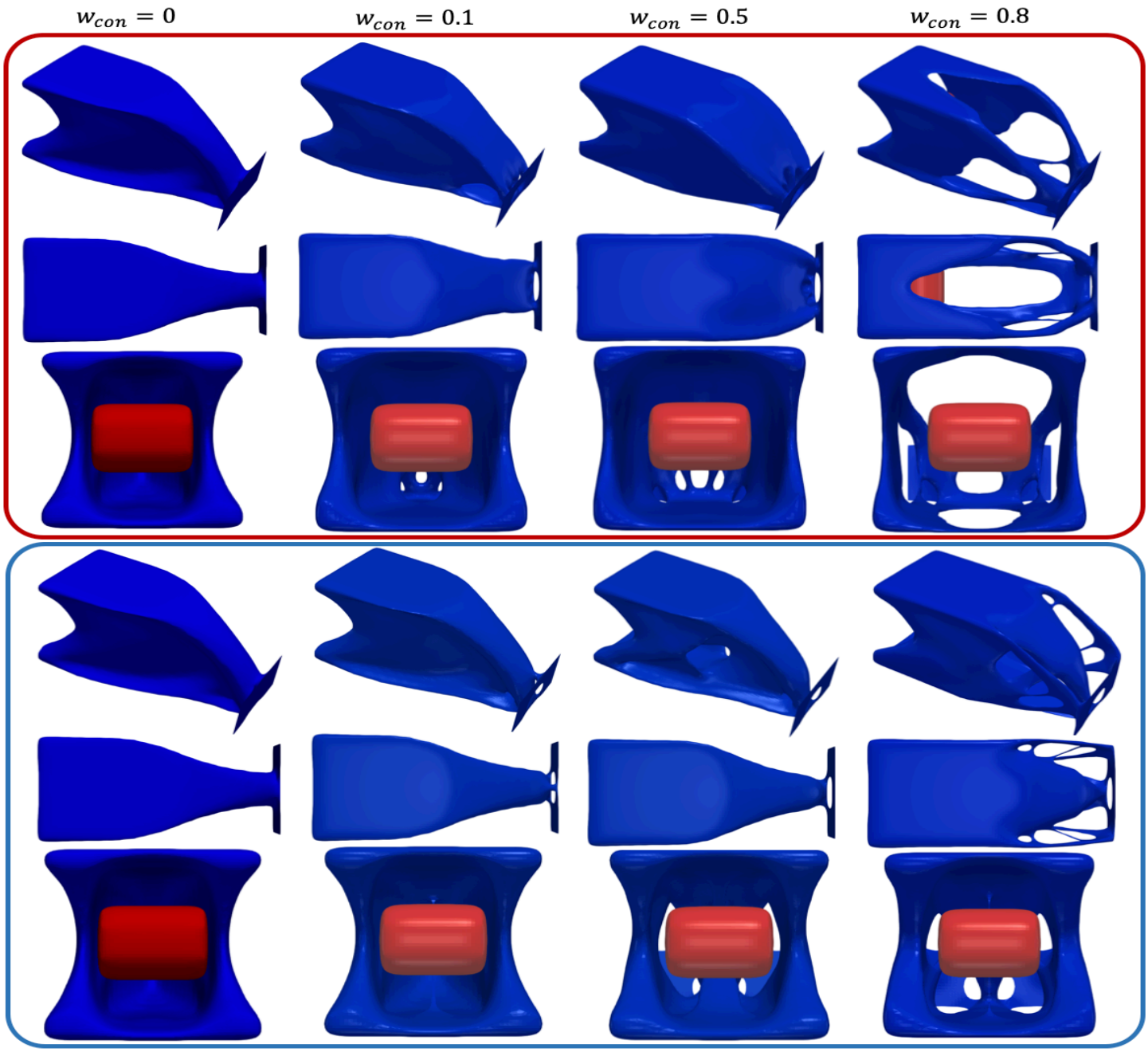


FIGURE 15: Results of 3D to with varying weights of connectivity enforcement in the TO loop. The top group (red border) corresponds with CSC constrained with structural compliance while the bottom group (blue border) corresponds with CSC constrained via thermal compliance. Blue material corresponds to the structure, red to the inactive cylinder, and white to void.

Similar to the 2D results, the 3D cantilevered beam demonstrates the effectiveness of our approach for enforcing CSC regardless of virtual physics. Without considering the connectivity enforcement the inlets and outlet are not connected. At low connectivity weights, connectivity is immediately enforced between inlet and outlet as seen by Fig. 15. Qualitatively, it appears that the openings and pathways become wider and wider as the connectivity weight is increased. This feature could be important to consider if wire thickness must be considered. Once again, the normalized compliance relative to the compliance of the unconstrained and unprocessed structure, c_0, for all the structures is provided by Tab. 4. Additionally, the compliance was computed for a structure in which a direct path between inlet and outlet was introduced after initial generation for $w_{\text{con}} = 0$.

© 2021 by ASME

	c/c_0
$w_{con} = 0$, No post-process	1.00
$w_{con} = 0$, Post-process	3.55
$w_{con} = 0.1$, Structural	1.46
$w_{con} = 0.1$, Thermal	1.04
$w_{con} = 0.5$, Structural	1.62
$w_{con} = 0.5$, Thermal	1.25
$w_{con} = 0.8$, Structural	2.03
$w_{con} = 0.8$, Thermal	1.30

TABLE 4: Normalized compliance results for the three generated topologies in 3D.

Table 4 once again demonstrates that considering connectivity in the design loop results in more optimal results than if connectivity were enforced by post processing. The decrease in performance is less in 3D because more material paths can be formed when compared to 2D. Importantly the results show that the optimized designs that consider the connectivity constraint are more complex than intuitive modifications done with post-processing.

As discussed previously, the manner in which connectivity was enforced has a few things in common with how the authors incorporated other manufacturing constraints in previous work [19], in that the global constraints such as accessibility and connectivity are recast into locally evaluable and differentiable forms, leading to sensitivity fields that can be used to guide TO. As a precursor to potential future work, a demonstration of the composability of manufacturing constraints is provided.

For example, consider a case where both accessibility and CSC constraints are considered simultaneously. The example is the same as that of Fig. 11, but an additional constraint is added that ensures all material is accessible for a cutter which approaches a block of raw material from any of the four boundaries. For more details on how accessibility is considered in the design loop see Mirzendehdel et al [19].



FIGURE 16: Resulting geometry of a cantilevered structure when connectivity is enforced (left) and when connectivity and accessibility are enforced (right). Black indicates dense elements, white indicates active void elements, and grey elements are inactive void elements.

As can be seen from Fig. 16, when accessibility is considered along with CSC, the design once again drastically changes. All internal structures are eliminated to ensure the material is accessible, but the structure has a similar boundary to enforce the CSC constraint. This example is a clear indication that the general framework shown in Fig. 3 shows promise for accommodating and composing a variety of manufacturing constraints. Future work may include validating this promise with more complex 2D and 3D examples and various combinations of manufacturing constraints.

5. CONCLUSION AND FUTURE WORK

In this paper a method for enforcing the connectivity between two points/regions over the complement space of a part was introduced, motivated by a need to enforce connectivity of embedded components. Then enforcement of connectivity was recast into a "virtual" compliance minimization problem where the precise selection of Neumann and Dirichlet boundary conditions at the desired inlets and outlets enforce the path-connectivity of two regions within the complement space. The introduced approach builds on previous work that utilized only Dirichlet boundary conditions that does not enforce connectivity between any two points of interest. More importantly, we demonstrated an effective approach to compose the CSC constraint with physics-based and (potentially) manufacturing constraints of different kinds within iterative TO.

After performing a parameter study of the approach to understand its capabilities and behavior, we integrated it into various structural compliance minimization problems in both 2D and 3D to show how CSC can be enforced. Importantly, the CSC constrained results were compared to the results of naïve post-processed connection of inlets to outlets. The results indicated that considering connectivity while optimizing for structural compliance resulted in stiffer structures compared to post-process corrections. Future work should focus on demonstrating connectivity for a variety of TO domains in 2D and 3D beyond minimizing structural compliance.

Additionally, the location of the inlets and outlets was defined *a priori* but one can easily encounter domains where the best choice for inlet and outlets positions is unclear. Future work should investigate how to actively determine the best location for inlets and outlets in the design loop.

Determining the optimal weightings of the primary and virtual problem is another area of future work. While we demonstrated small weighting can enforce CSC, without drastically impacting performance, the geometry of the connected pathways may not be sufficiently wide for internal wiring or powder removal. By changing the weighting, the size of the pathways, generally, increases which may be desirable. Providing the designer with a systematic approach for selecting the proper weighting based off their needs would be desirable.

From a broader view, the manner in which connectivity was imposed is similar to how other manufacturing constraints can and have been imposed. The constraints are recast into a locally differentiable functions whose sensitivities can augment the primary objective function. In general, this procedure can be repeated for a multitude of constraints creating a general workflow for TO. A simple example of composing connectivity and accessibility within TO was provided to demonstrate the capabilities of the workflow. As more manufacturing constraints are recast locally, they can be seamlessly integrated into a single generative workflow for part design.

© 2021 by ASME

ACKNOWLEDGEMENTS

This research was developed with funding from the Defense Advanced Research Projects Agency (DARPA). The authors would also like to thank Sai Nelaturi for his technical advice. The views, opinions and/or findings expressed are those of the authors and should not be interpreted as representing the official views or policies of the Department of Defense or U.S. Government.

REFERENCES

[1] Bendsoe, M. P., and Sigmund, O., 2013, *Topology Optimization: Theory, Methods, and Applications*, Springer Science & Business Media.

[2] Sigmund, O., and Maute, K., 2013, "Topology Optimization Approaches," Struct. Multidiscip. Optim., **48**(6), pp. 1031–1055.

[3] Allison, J., Sharpe, C., and Seepersad, C. C., 2019, "Powder Bed Fusion Metrology for Additive Manufacturing Design Guidance," Addit. Manuf., **25**, pp. 239–251.

[4] Jiang, J., Xu, X., and Stringer, J., 2018, "Support Structures for Additive Manufacturing: A Review," J. Manuf. Mater. Process., **2**(4), p. 64.

[5] Rosen, D. W., Seepersad, C. C., Simpson, T. W., and Williams, C. B., 2015, "Design for Additive Manufacturing: A Paradigm Shift in Design, Fabrication, and Qualification," J. Mech. Des., **137**(11).

[6] Jiang, J., Lou, J., and Hu, G., 2019, "Effect of Support on Printed Properties in Fused Deposition Modelling Processes," Virtual Phys. Prototyp., **14**(4), pp. 308–315.

[7] Kumbhar, N. N., and Mulay, A. V., 2018, "Post Processing Methods Used to Improve Surface Finish of Products Which Are Manufactured by Additive Manufacturing Technologies: A Review," J. Inst. Eng. India Ser. C, **99**(4), pp. 481–487.

[8] Savage, V., Schmidt, R., Grossman, T., Fitzmaurice, G., and Hartmann, B., 2014, "A Series of Tubes: Adding Interactivity to 3D Prints Using Internal Pipes," *Proceedings of the 27th Annual ACM Symposium on User Interface Software and Technology*, pp. 3–12.

[9] Zhou, M., Lazarov, B. S., Wang, F., and Sigmund, O., 2015, "Minimum Length Scale in Topology Optimization by Geometric Constraints," Comput. Methods Appl. Mech. Eng., **293**, pp. 266–282.

[10] Mirzendehdel, A. M., and Suresh, K., 2016, "Support Structure Constrained Topology Optimization for Additive Manufacturing," Comput.-Aided Des., **81**, pp. 1–13.

[11] Langelaar, M., 2016, "Topology Optimization of 3D Self-Supporting Structures for Additive Manufacturing," Addit. Manuf., **12**, pp. 60–70.

[12] Qian, X., 2017, "Undercut and Overhang Angle Control in Topology Optimization: A Density Gradient Based Integral Approach," Int. J. Numer. Methods Eng., **111**(3), pp. 247–272.

[13] Mirzendehdel, A. M., Rankouhi, B., and Suresh, K., 2018, "Strength-Based Topology Optimization for Anisotropic Parts," Addit. Manuf., **19**, pp. 104–113.

[14] Vantyghem, G., Boel, V., De Corte, W., and Steeman, M., 2018, "Compliance, Stress-Based and Multi-Physics Topology Optimization for 3D-Printed Concrete Structures," *RILEM International Conference on Concrete and Digital Fabrication*, Springer, pp. 323–332.

[15] Langelaar, M., 2019, "Integrated Component-Support Topology Optimization for Additive Manufacturing with Post-Machining," Rapid Prototyp. J.

[16] Liu, S., Li, Q., Chen, W., Tong, L., and Cheng, G., 2015, "An Identification Method for Enclosed Voids Restriction in Manufacturability Design for Additive Manufacturing Structures," Front. Mech. Eng., **10**(2), pp. 126–137.

[17] Li, Q., Chen, W., Liu, S., and Tong, L., 2016, "Structural Topology Optimization Considering Connectivity Constraint," Struct. Multidiscip. Optim., **54**(4), pp. 971–984.

[18] Gaynor, A. T., and Guest, J. K., 2016, "Topology Optimization Considering Overhang Constraints: Eliminating Sacrificial Support Material in Additive Manufacturing through Design," Struct. Multidiscip. Optim., **54**(5), pp. 1157–1172.

[19] Mirzendehdel, A. M., Behandish, M., and Nelaturi, S., 2020, "Topology Optimization with Accessibility Constraint for Multi-Axis Machining," Comput.-Aided Des., **122**, p. 102825.

[20] Wasserfall, F., Hendrich, N., Ahlers, D., and Zhang, J., 2020, "Topology-Aware Routing of 3D-Printed Circuits," Addit. Manuf., **36**, p. 101523.

[21] Hart, P. E., Nilsson, N. J., and Raphael, B., 1968, "A Formal Basis for the Heuristic Determination of Minimum Cost Paths," IEEE Trans. Syst. Sci. Cybern., **4**(2), pp. 100–107.

[22] Bendsøe, M. P., and Sigmund, O., 1999, "Material Interpolation Schemes in Topology Optimization," Arch. Appl. Mech., **69**(9), pp. 635–654.

[23] Svanberg, K., 1987, "The Method of Moving Asymptotes—a New Method for Structural Optimization," Int. J. Numer. Methods Eng., **24**(2), pp. 359–373.

 © 2021 by ASME